Iowa State University

From the SelectedWorks of Nicole N. Hashemi

2010

Dynamic reversibility of hydrodynamic focusing for recycling sheath fluid

Nicole N. Hashemi, *Naval Research Laboratory*
Peter B. Howell, Jr., *Naval Research Laboratory*
Jeffrey S. Erickson, *Naval Research Laboratory*
Joel P. Golden, *Naval Research Laboratory*
Francis S. Ligler, *Naval Research Laboratory*

Dynamic reversibility of hydrodynamic focusing for recycling sheath fluid†

Nastaran Hashemi, Peter B. Howell, Jr., Jeffrey S. Erickson, Joel P. Golden and Frances S. Ligler*

The phenomenon of "unmixing" has been demonstrated in microfluidic mixers, but here we manipulate laminar flow streams back to their original positions in order to extend the operational utility of an analytical device where no mixing is desired. Using grooves in the channel wall, we passively focus a sample stream with two sheath streams to center it in a microchannel for optical analysis. Even though the sample stream is completely surrounded by sheath fluid, reversing the orientation of the grooves in the channel walls returns the sample stream to its original position with respect to the sheath streams. We demonstrate the separation of the sample stream from the contiguous sheath streams and the recycling of the sheath fluid using the reversibility of laminar flow. Polystyrene microspheres and fluorescent dye were used to quantify the performance of the unsheathing process. We found that the maximum numbers of microspheres and all of the fluorescent dye were recaptured at sheath recycling levels <92%. The use of this sheathing technique has previously been demonstrated in a sensitive microflow cytometer; the unsheathing capability now provides the opportunity to recover particles from the sensor with minimal dilution or to recycle the sheath fluid for long-term unattended operation.

Introduction

Laminar flow characteristics in microchannels have both facilitated and frustrated the development of lab-on-a-chip systems. Many microfluidic devices, especially those intended as mixers, are operated in the creeping flow limit; in this regime flows are dominated by viscosity and inertia plays a marginal role. Stroock *et al.* used herringbone grooves on the floor of the microchannel to generate transverse flows and to increase the diffusive mixing between adjacent streams.[1,2] The effect of chaotic advection in microchannels with the grooves was numerically investigated by Wang *et al.*[3]

On the other hand, hydrodynamic focusing of one laminar stream by another without mixing has inspired new approaches for separations, optical components, biosensors, and cell analysis.[4–8] In nearly all of these publications, laminar flow is used to alter a flow stream irreversibly or redistribute components within parallel flow streams without chaotic advection. The reversibility of these processes has received little attention. Here we demonstrate the capacity of hydrodynamic focusing to encircle a sample stream completely with a sheath fluid, reduce the diameter of the sample stream (as for cytometry), and then reverse the process both to recapture sample components with minimal dilution and to recycle the sheath fluid.

Nonlinear periodic or chaotic dynamics are inherently irreversible.[9] However, at low Reynolds number, the dynamics of fluids can be reversed by reversing the direction of the forces applied to the system.[10–15] In microfluidic devices, flows are mainly dominated by viscosity, and inertia plays a marginal

role. The equations of motion in viscosity-dominated flows are linear and do not depend explicitly on time. In his classic video clip, Taylor[12] demonstrated that a drop of dye added to a viscous fluid between two cylinders could be stretched by rotating the outer cylinder and reconstituted by reversing the direction of rotation. Heller also demonstrated unmixing by reversal of motion while observing thermal agitation of molecules.[16] Recently, Fuerstman *et al.*[10] investigated reversibility to encrypt and decrypt information. Sundararajan *et al.* investigated the reversibility of convection–diffusion in laminar chaotic flows in a patterned microchannel.[4] While continuing to pump two fluids in the same direction, Howell *et al.* observed that symmetrical grooves in the walls of microfluidic channels would both create and reverse movements of two fluids across a channel, to bring the two streams back to their original positions.[18,19] He used this observation to eliminate all pairs of symmetrical grooves in a passive mixer, reducing the length and complexity of a mixing channel, without reducing effectiveness of mixing. Tan *et al.* proposed using alternating mirror-image sets of herringbone grooves pointing up and down the channel to enhance chaotic advection and to improve diffusive mixing.[17] The authors failed to realize that reversing the grooves would not enhance chaotic advection under laminar flow conditions.[18] They used low viscosity fluids in channels of 2.0×0.4 mm, with a linear velocity sufficiently slow to allow diffusive mixing independent of any chaotic advection. Furthermore, they only showed improved mixing compared to channels without grooves and not compared to channels with no reversed grooves.

Control of flow streams using grooves[20] has recently been used to develop very sensitive microflow cytometers.[8,21] The grooves in the channel wall direct the sheath fluid completely around the core (sample) stream. This hydrodynamic positioning, along with control of the relative flow rates of the sheath and sample streams, focuses the sample stream as it crosses the laser beams in the interrogation region to generate three-color fluorescence and

Center for Bio/Molecular Science and Engineering, Naval Research Laboratory, Washington, DC, USA. E-mail: Frances.ligler@nrl.navy.mil; Tel: +1 202-404-6002

† Electronic supplementary information (ESI) available: Includes micrographs of fluorescent streams passing through the sheathing and unsheathing grooves (A1) and exiting the outlet channel with varying percentages of sheath recycling (A2). See DOI: 10.1039/c004696e

light scatter signals. The data obtained in a six-target assay using the microflow cytometer were equivalent to data obtained using a commercial benchtop cytometer.[21] However, the impetus for miniaturization is more a function of potential cost reduction and utility outside the laboratory than expected increases in sensitivity. The capacity for recycling the sheath fluid would reduce the logistical burden for on-site and point-of-care applications in terms of volumes for sheath fluid reservoirs and periods of time between replenishment, while the ability to recapture cells after analysis without dilution could facilitate cell recapture for subsequent laboratory analyses. Here we describe the use of hydrodynamic focusing both to focus the sample stream in two dimensions using sheath fluid and subsequently to separate the sample stream from the surrounding sheath fluid. This hydrodynamic process thus provides sheath fluid uncontaminated with sample for reuse and minimally diluted sample for further analysis.

Experimental

A flow channel was manufactured in polydimethylsiloxane (PDMS) using standard soft lithography[22] with a groove design already proven to focus the sample stream in the center of the channel for the microflow cytometer.[20] Fluidic inlets were cored into the top of the PDMS module. Silicone tubing (Cole-Parmer Instrument Company, Vernon Hills, IL) with an internal diameter of 760 μm was connected to the inlets. Channel dimensions were 390 μm wide by 130 μm deep. The chevron-shaped grooves were 100 μm wide by 65 μm deep and intersected the channel wall at 45 degrees. The design included four grooves used for sheathing and four reversed grooves used for unsheathing (as shown in Fig. 1).

Sheath flow with a fixed flow rate of 1100 μL min⁻¹ was introduced on both sides of the sample stream using a bifurcated tube extending from a single reservoir (Fig. 2). A precise bi-directional speed-control peristaltic pump (P625/66.143, Instech Laboratories, Inc., Plymouth, PA) was used for this purpose. Typically, the flow from this type of pump suffers from a strong pulse whenever a roller leaves the tube track. We used a pulse
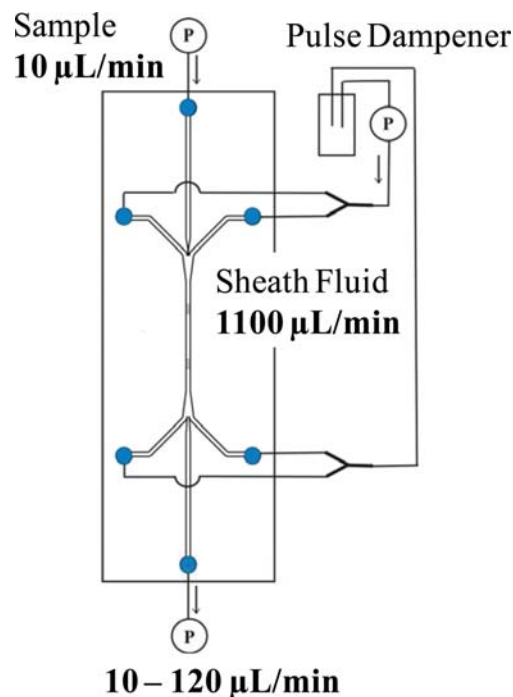

Fig. 2 Schematic of experimental setup. A single peristaltic pump pulled the sheath fluid out of the channel from both sides, recirculating it back into the channel on both sides of the sample inlet. Sample was introduced into and drawn out of the channel using separate syringe pumps.
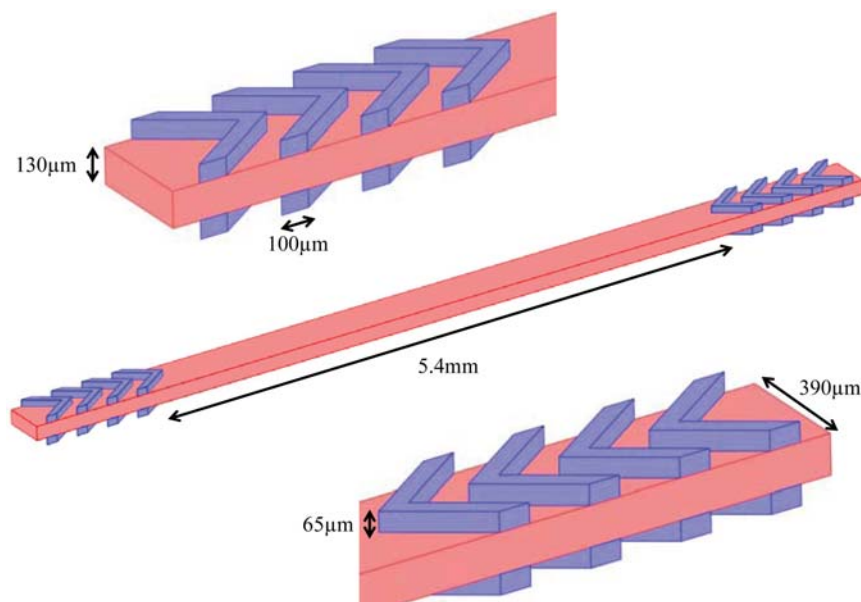

Fig. 1 Schematic of top half of the microchannel. The length, width and depth of the channels are 15.2 mm, 390 μm and 130 μm, respectively. The chevron-shaped grooves are 100 μm wide by 65 μm deep and intersect the channel wall at 45 degrees. The distance between the sheathing and unsheathing chevron structures is 5.4 mm.

dampener to prevent the pulsation caused by the peristaltic pump. The pulse dampener consisted of a 50 mL reservoir containing 3 mL of deionized water. At the sheath flow rate of 1100 μL min⁻¹, about 3 minutes was required for the system to achieve a steady constant flow rate. To minimize displacement of the sample stream across the channel, a Y connection was used to split the sheath flow into the two sheath fluid channels, and sheath fluid was introduced into both sides of the channel using one pump. Sample was introduced into and drawn out of the channel using syringe pumps (EW-74900-10, Cole-Parmer Instrument Company, Vernon Hills, IL). The inlet flow rate of the sample fluid is fixed at 10 μL min⁻¹. However, the sample outlet flow rate from the central outlet varied from 10 μL min⁻¹ to 120 μL min⁻¹, with increments of 11 μL min⁻¹, providing recycled sheath fluid of 100% to 90%.

Since the sheath flow is introduced into the channel with a fixed flow rate, the sheath fluid stored in the pulse dampener compensated for the loss of sheath fluid out of the central outlet. In other words, we lost some of the stored water over the course of the experiment, but the flow rate of the sheath fluid at the inlet remained constant.

The chevron-shaped grooves performed the sheathing by moving some of the sheath fluid above and below the sample stream. To reverse the sheathing, a second set of chevron-shaped grooves was placed in the channel pointing upstream, *i.e.* symmetrical to the first set with an axis of symmetry across the middle of the channel. The sheath fluid flowed out of the channel from outlets on both sides of the central core outlet, collected in the reservoir of excess sheath fluid used as a pulse dampener, and recirculated back into the channel on both sides of the sample inlet. In order to vary the volume of sheath fluid recycled, relative to the volume of sheath fluid introduced, pumps were placed at both the center inlet and center outlet. Increasing the flow rate of the exit sample stream pump relative to the inlet pump caused sheath fluid as well as sample fluid to be removed from recirculation. To accommodate fluctuations (caused by unbalanced fluid pumping or bubbles) that would cause the sample to move from the center of the channel, the center outlet channel was the same width as the two sheath outlet channels.

Results and discussion

A Nikon Eclipse TE2000U inverted microscope was used to image the microchannel. The chip was placed on the microscope platform while connected to the pumps. Fig. 3(A) shows an image of the microfluidic channel at a sheath flow rate of 1100 μL min⁻¹ and inlet sample flow rate of 10 μL min⁻¹. In this experiment, fluids were permitted to flow freely out of the outlet channels and the amount of sheath fluid in the central outlet channel was simply a function of the relative widths of the three outlet channels. The fluorescent sample fluid enters the channel between the two sheath inlets and exits between the two sheath outlets.

Fluid modeling was used for optimization and analysis of a microchannel with the specifications used experimentally. To describe the Lagrangian diffusive transport in the microchannel, we used the COMSOL Multiphysics finite element analysis package. Navier–Stokes equations for incompressible flow at steady state were used to numerically solve for the continuity and the momentum balance.

$$(\boldsymbol{u}\cdot\nabla)\boldsymbol{u} = -\frac{1}{\rho}\nabla p + \nu\nabla^2\boldsymbol{u} \tag{1}$$

$$\nabla\cdot\boldsymbol{u} = 0$$

Here ∇ is the divergence operator, ρ represents density, $\boldsymbol{u}$ is the velocity vector, p is the pressure, and ν is the kinematic viscosity. Since the inertial forces are negligible at low Reynolds number, the motion of the fluid can be approximately described by the reversible Stokes equation in which the nonlinear term can be neglected.[10,23] Zero-slip boundary condition was assumed for all surfaces.

To describe the diffusive transport in the microchannel, Fick's law was used.

$$-\nabla\cdot(-D\nabla c + c\boldsymbol{u}) = 0 \tag{2}$$

D is the diffusion coefficient and c represents the concentration. Assuming that a change in concentration does not affect the viscosity and density of the fluid, we solved the Navier–Stokes equations first and then solved for the convection–diffusion phenomena. We took advantage of the symmetry of the design and simulated only one quadrant of the channel to reduce the computation time. A diffusion coefficient of $D = 1 \times 10^{-10}$ m² s⁻¹ was used for the dye in the mass-transport simulations. The Stokes–Einstein equation was used to calculate the diffusion coefficient for isolated Brownian spheres

$$D = \frac{K_B T}{6\pi\eta R_p} \tag{3}$$

where the Boltzmann's constant $K_B = 1.38 \times 10^{-23}$, $T = 300$ K, radius of the sphere $R_p = 2.5 \times 10^{-6}$ m, and dynamic viscosity of buffer $\eta = 0.001$ N s m⁻². The diffusion coefficient for 5 micron spheres was found to be 8.8×10^{-14} m² s⁻¹.

The simulation in Fig. 3(B) depicts the positions of the sheath and sample streams at different cross-sections throughout the channel at a sheath flow rate of 1100 μL min⁻¹ and an inlet sample flow rate of 10 μL min⁻¹. In this simulation, fluids were permitted to flow freely out of the outlet channels and the amount of sheath fluid in the central outlet channel was simply a function of the relative widths and geometry of the three outlet channels. The flow rate exiting freely out of the central outlet channel was 85 μL min⁻¹ consisting of all the sample flow (10 μL min⁻¹) and 75 μL min⁻¹ of sheath fluid. This is identical to the 93% sheath recycling using a pump to draw the flow out of the central outlet channel. The diffusive transport calculations indicate the diffusion of Rhodamine WT dye (Bright Dyes, Miamisburg, OH) from the sample stream into the sheath stream.

The simulations indicated that the sample stream was completely surrounded by the sheath stream after passing the first set of chevrons. At the flow rates utilized, diffusion was limited as the sample stream passed down the channel. After passing through the reverse chevrons, the sample stream returned most of the way to the top and bottom of the channel, with diffusion preventing a complete return to the narrow stream width exhibited at the entrance.
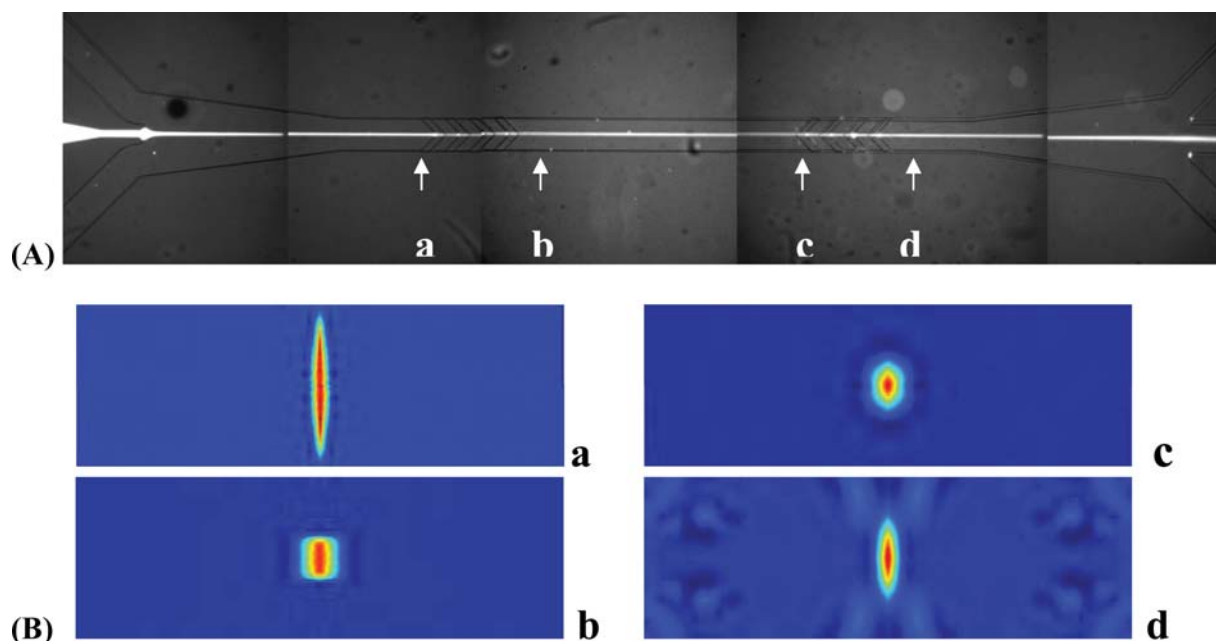
Fig. 3 (A) The photocomposite image of the microfluidic channel shows the fluorescent sample fluid entering the channel between the two sheath inlets and exiting between the two sheath outlets. Note that the fluorescence appears dimmer between the sets of chevrons where the sample stream does not reach the top of the channel. A close-up image of the chevrons is supplied in ESI† (Fig. A1). (B) Simulation showing concentration distribution for low molecular weight components in the sample steam (*e.g.* dye) at a sheath (blue) and sample (red) inlet flow rates of 1100 and 10 μL min⁻¹, respectively. The cross-sections in the simulation were selected at positions that correspond to the locations in the actual microchannel as marked in the micrograph: (a) before inlet chevrons, (b) after inlet chevrons, (c) before reverse chevrons, and (d) after reverse chevrons.

Confocal microscopy (Nikon Eclipse TE2000E inverted confocal microscope) verified that the stream was pushed away from the top of the channel between the chevrons and returned to a position near the channel top after the reversed chevrons. The micrographs also verify that the sample stream remained centered in the channel without significant mixing or diffusion (Fig. 4). The sample size with concentration larger than 0.4 (where the undiluted dye solution has a fluorescence intensity of 1 and sheath is 0) was found to be 12.6 μm (width) × 93.7 μm (height) at point a, 31.6 μm (width) × 56.3 μm (height) at point b, 29.5 μm (width) × 45.8 μm (height) at point c, and 11.5 μm (width) × 61 μm (height) at point d.

Limits of reversibility

Since this paper focuses on the performance of the reversibility, we will not report the various iterations of the geometries that we explored. For the current design, we investigated the range of Reynolds numbers for which the reversibility holds. The numerical simulations were carried out for a large range of Reynolds number. Fig. 5 shows the upper right quarter of the cross-section of the channel. In this figure, the inlet sample width and height are 20 μm and 65 μm, respectively, since the COM-SOL simulations represent only one quadrant of the channel. The actual initial width and height of the entrance channel for the sample stream are 40 μm and 130 μm. The distance between the sheathing and unsheathing chevron structures is 5.4 mm. The results show that for the current geometry the reversibility is applicable for 12 < *Re* < 100. For Reynolds number below 12, as the core stream (dye) width is relatively large after passing the inlet chevrons, dye diffuses into the sheath stream on the corner

of the channel after the flow passes the outlet chevrons. However, most of the dye remains in the center of the channel. For Reynolds number above 100, the process of encircling the core stream with the sheath fluid does not occur efficiently and the core stream diffuses to the top and bottom of the channel instead of the center after passing the inlet chevrons.

Dark blue represents the sheath flow with assigned concentration of 0 and red represents sample flow (dye) with a maximum concentration of 1. Initially starting with a width of 40 μm and height of 130 μm, the sample fluid becomes thinner and shorter even before passing the inlet (folding chevrons) at point a. However, the height of the sample fluid after passing the inlet chevrons becomes 34 μm regardless of the Reynolds number while the width of the sample fluid shows dependency on the flow-rate ratio. Fig. 6 shows the width and height of a rectangle containing the region with concentration of larger than 0.4 at point d (after reverse chevrons). As the Reynolds number increases, the width and height of the core after passing through the reverse chevrons decrease until the Reynolds number is too high (>100) to maintain the discrete flow streams. From the experiment, the dimensions of the sample stream with concentration larger than 0.4 at point d was found to be 11.5 μm (width) × 61 μm (height) while the numerical simulation showed a 19 μm (width) × 67 μm (height) sample size. Given the limitations of measuring the fluorescence of the sample stream, these values are in excellent agreement.

Performance assessment

To quantify the reversibility, we included a low molecular weight fluorescent dye and 5 μm polystyrene microspheres (PP-50-10,
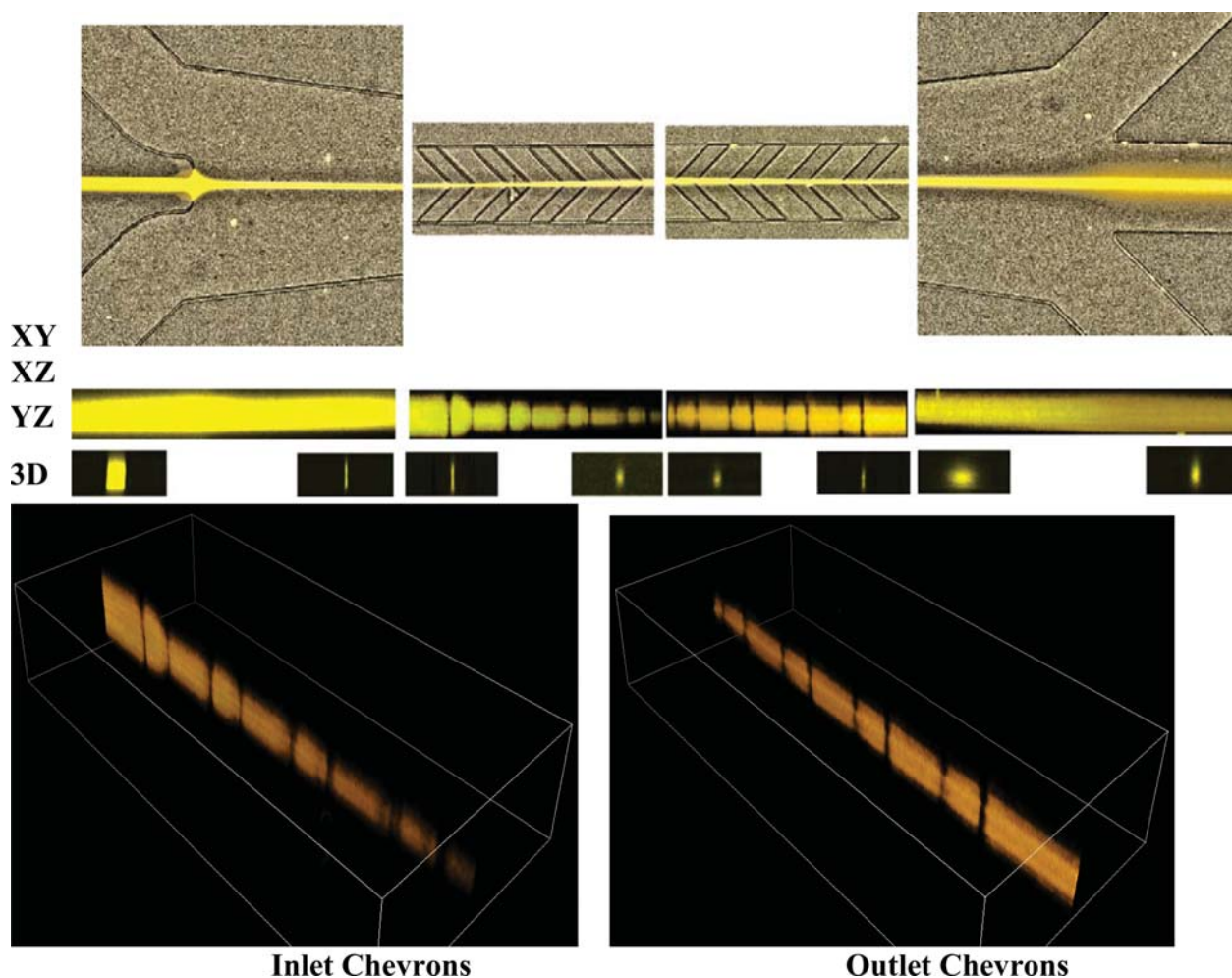
Fig. 4 Confocal microscopy images of the sheathing and unsheathing processes at 90% sheath fluid recycling. XY: top view of the inlet, inlet chevrons, reverse chevrons, and outlet sections of the microchannel. XZ: side view of the same sections. YZ: cross-section views at upstream and downstream edges of each of the sections in the XY and XZ panels directly above. 3D: constructed images of the sample fluid at the inlet and reverse chevrons. The sample height decreases upon passing through the inlet chevrons and increases by passing through each reverse chevron. The inlet sample flow rate is 10 μL min⁻¹ and the sheath flow rate is 1100 μL min⁻¹. The outlet sample flow rate is 120 μL min⁻¹.

Spherotech, Inc., Lake Forest, IL) in the sample stream. The microspheres were diluted in a solution of bovine serum albumin (BSA) in deionized water. The final concentration of the microspheres was 400 microspheres per μL. BSA was used to prevent aggregation of the microspheres in the sample stream. The hydrophobicity of the microspheres caused some loss due to sticking in the inlet tubing. We collected 1 mL of the sample drawn from the sample outlet channel and measured the recovery of the fluorescent dye and microspheres as they exited the center outlet channel (Fig. 4 (XY)). The concentration of fluorescent dye exiting the center outlet channel was quantified using a full-spectrum UV/Vis spectrophotometer and was compared to the dye concentration entering the center inlet. The UV/Vis spectrophotometer was calibrated based on the absorbance for both 260 nm and 567 nm wavelengths for the inlet sheath fluid.

The product of absorbance and volumetric flow rate was used to quantify recycling efficiency. The nondimensional ratio of this product at the outlet sample and inlet sample provides an indication of recycling performance.

$$\text{Recycling efficiency} = \frac{(QA)_{\text{inlet sample}}}{(QA)_{\text{outlet sample}}} \quad (4)$$

Q is the volumetric flow rate and A is absorbance at 567 nm.

To count the polystyrene microspheres, we used an Accuri C6 flow cytometer (Accuri Cytometers, Inc., Ann Arbor, MI). The number of microspheres exiting the center channel was reported as a percentage of the maximum recoverable microspheres after passage through the device (370 microspheres per μL at 83% sheath recycling). The 83% sheath recycling clearly focused the entire stream into the middle of the center outlet channel as visualized using fluorescence microscopy.

Letting both sheath and sample fluids flow freely out of the outlet channels, the flow rate for the central outlet channel was measured to be 85 μL min⁻¹ (consisting primarily of sample flow with a small amount of sheath fluid) and the flow rate from each of the adjacent outlets was 75 μL min⁻¹ (sheath fluid only). Note that 85 μL min⁻¹ is the same flow rate as was used to provide 93%
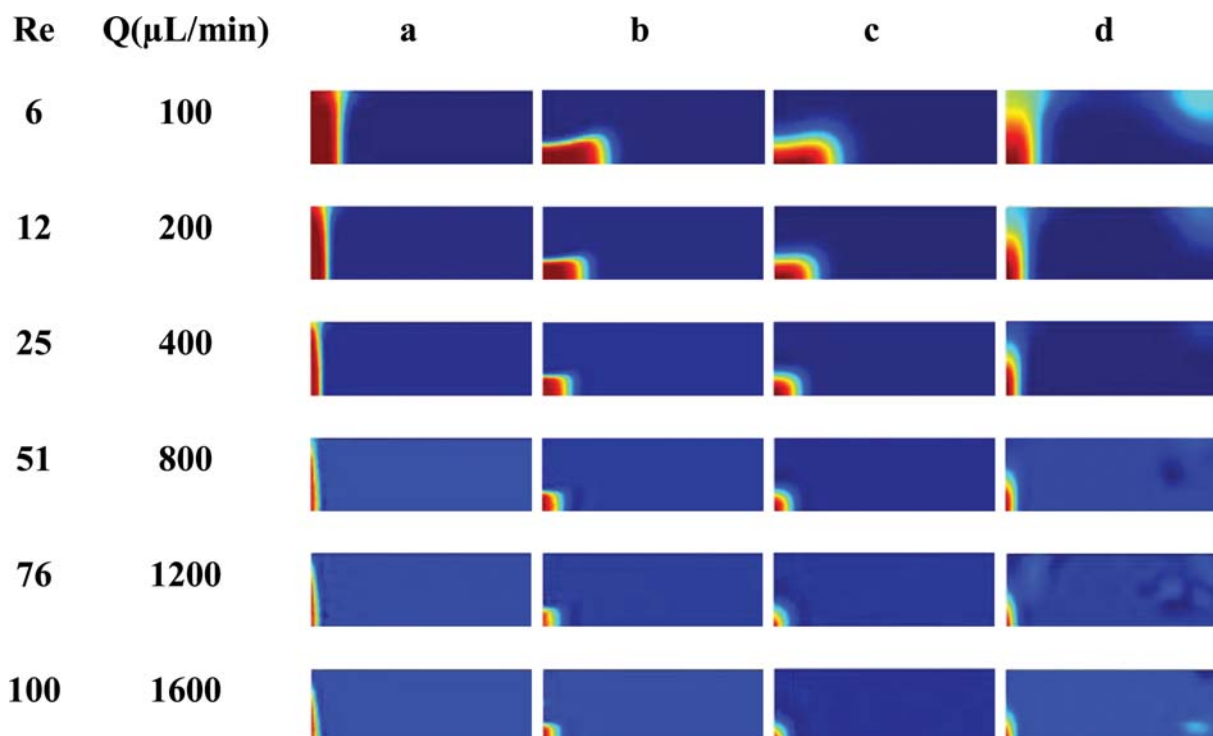
Fig. 5 Concentration distribution for low molecular weight components in the sample steam for sheath (blue) and sample (red). (a) before inlet chevrons, (b) after inlet chevrons, (c) before reverse chevrons, and (d) after reverse chevrons. Sheath flow rates (Q) were varied at 100 µL min^{-1} ($Re = 6$), 200 µL min^{-1} ($Re = 12$), 400 µL min^{-1} ($Re = 25$), 800 µL min^{-1} ($Re = 51$), 1200 µL min^{-1} ($Re = 76$), and 1600 µL min^{-1} ($Re = 100$). The core flow rate was constant at 10 µL min^{-1}.

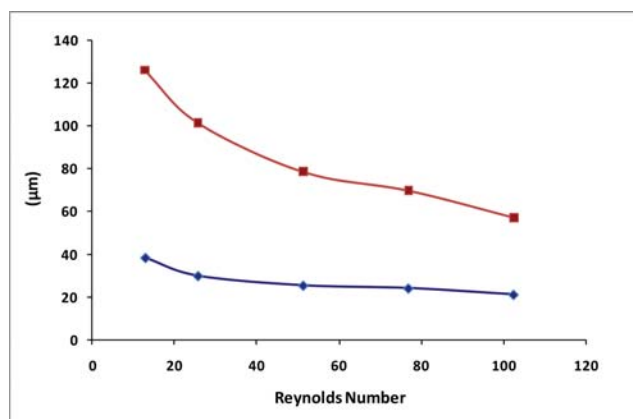**Fig. 6** Height (—□—) and width (—◇—) of the sample fluid after passing through the reverse chevrons (position d in Fig. 3(A) and Fig. 5) obtained using COMSOL simulations of the channel photographed in Fig. 3(A). Initial height and width of the entrance channel for the sample stream are 130 µm and 40 µm.

sheath recycling. Drawing the flow out of the central channel with a higher flow rate (resulting in more sheath fluid in the central channel and less sheath fluid captured in the adjacent outlets for recycling) guaranteed recapture of maximum numbers of microspheres, since all of the sample stream was effectively centered in the center outlet channel.

As the proportion of fluid drawn out of the center of the microchannel increased, the recovery of the fluorescence and microspheres increased. Since the system was a closed loop, drawing the sample stream out of the channel with a faster flow rate than that used to pump sample into the channel reduced the volume of sheath fluid recycled.

All of the fluorescent dye, and thus 100% of the sample stream, was recovered when the system was operated with ≤90% sheath recycling (Fig. 7(a)). For detailed images of the sample stream recapture, see Fig. A2 in the ESI†. The percentage of sheath that must be recaptured in order to recapture all of the sample stream is primarily a function of pump pulsation. In a perfect world, to recapture 100% of the sample stream, the only factor affecting the flow rate at which the sample is pulled out of the central outlet, and correspondingly, the amount of sheath fluid included, would be a function of the diffusion occurring between the sample inlet and outlet over the length of the channel at the flow rate used.

The maximum number of microspheres (~80%) was recaptured at sheath recycling levels ≥92% (Fig. 7(b)). At 90% sheath recycling, no microspheres were detected in the recycled sheath fluid, further supporting evidence that the failure to recapture all the input microspheres (beads) is a function of sticking to the walls of the inlet and outlet tubing and not to diffusion from the core into the sheath stream. At 83% sheath recycling, the flow rate and amount of sheath fluid in the outlet channel are both high enough that the microspheres are less likely to stick to the walls of the outlet tubing than at 92%.

Our results showing more facile recapture of the microspheres than dye are consistent with the observation that, at high Peclet
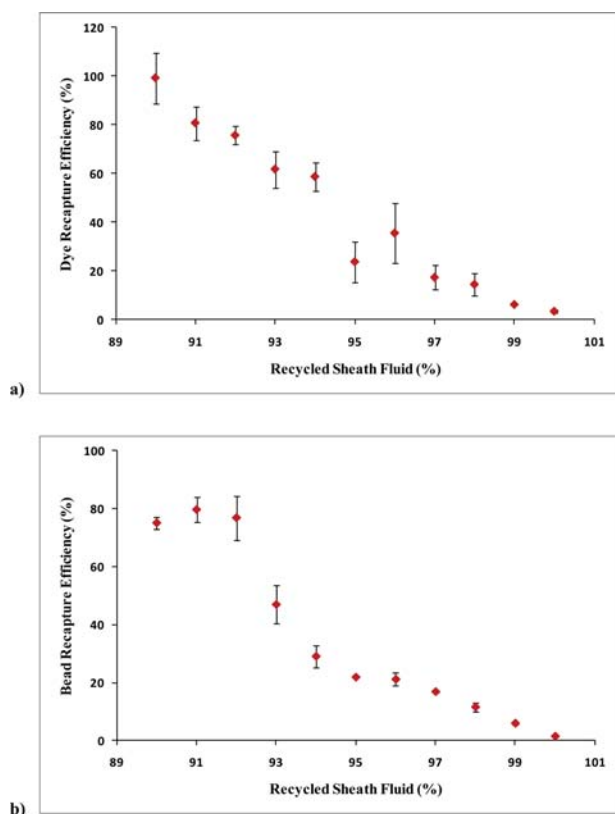
Fig. 7 (a) The percentage of the fluorescent dye recaptured increased as the proportion of sheath fluid recycled decreased. (b) The recovery of the 5 micron microspheres, compared to the 370 μL^{-1} recoverable at 83% sheath recycling, was maximized at $\leq$92% sheath recycling. Values in both graphs are the mean and standard deviation from 4 experiments; in some cases the standard deviations are small enough for the bars to be obscured by the markers for the mean.

numbers and low Reynolds numbers, small particles follow the fluid streamlines and travel along the average fluid flow direction. This is because, at low Re number, the inertial drift does not cause movement across streamlines.[24] In other words, we can recapture all the 5 μ microspheres without recapturing 100% of the core fluid.

In the device described here, the sheath flow folds over and under the sample flow with a small angle, enabling the reversibility of the laminar flows with the subsequent reverse chevron structures without chaotic advection or diffusive mixing. This effect only works with a given flow rate and a given distance between the folding and unfolding chevron structures. Experiments conducted at slower flow rates were less successful in recapturing dye and microsperes in the central outlet (data not shown). What is interesting (and is shown in Fig. 7) is that the recapture of microspheres is measurably more efficient than the recapture of dye molecules with faster diffusion constants. The latter was used to depict the recapture of the entire sample stream precisely because it represented a "worst case" situation for recycling.

Conclusions

This study demonstrates the reversibility of hydrodynamic focusing without chaotic advection in an analytical device. Using the reversibility in the laminar flow regime, we designed a microdevice that returns the sample stream to its original position with respect to the sheath streams. We quantified the reversibility by recapturing the microspheres as an indicator of particulates in a sample and a low molecular weight dye to visualize the exact position of the sample stream. We achieved 100% recapture of the sample stream and the recovered microspheres.

The reversibility of the hydrodynamic focusing has application for automated processing of cells and particles, for long-term unattended use of flow cytometers, and for improved cell recovery after sorting of tumor and stem cells. For example, cells could be mixed with more rapidly diffusing dyes and then recaptured in their original volume. Cytometers with recycled sheath fluid could be used to monitor recycled drinking water for bacterial contamination on the space shuttle or to reduce the size and logistical burden of systems that monitor the air for release of biothreat agents.[25] Finally, circulating tumor cells could be concentrated for culture or genetic analysis after identification by flow cytometry without immunomagnetic separation or centrifugation.[26]

Acknowledgements

References

1 A. D. Stroock, S. K. W. Dertinger, A. Ajdari, I. Mezic, H. A. Stone and G. M. Whitesides, *Science*, 2002, **295**(5555), 647–651.
2 A. D. Stroock, S. K. Dertinger, G. M. Whitesides and A. Ajdari, *Anal. Chem.*, 2002, **74**(20), 5306–5312.
3 H. Wang, P. Iovenitti, E. Harvey and S. Masood, *J. Micromech. Microeng.*, 2003, **13**, 801–808.
4 P. Sundararajan, J. Kirtland, D. Koch and A. Stroock, *American Physical Society, Division of Fluid Dynamics*, November 23–25, 2008.
5 A. Wolff, I. R. Perch-Nielsen, U. D. Larsen, P. Friis, G. Goranovic, C. R. Poulsen, J. P. Kutter and P. Telleman, *Lab Chip*, 2003, **3**, 22–27.
6 M. M. Wang, E. Tu, D. E. Raymond, J. M. Yang, H. Zhang, N. Hagen, B. Dees, E. M. Mercer, A. H. Forster, I. Kariv, P. J. Marchand and W. F. Butler, *Nat. Biotechnol.*, 2004, **23**, 83–87.
7 P. Yager, T. Edwards, E. Fu, K. Helton, K. Nelson, M. R. Tam and B. H. Weigl, *Nature*, 2006, **442**, 412–418.
8 J. P. Golden, J. S. Kim, J. S. Erickson, L. R. Hilliard, P. B. Howell, G. P. Anderson, M. Nasir and F. S. Ligler, *Lab Chip*, 2009, **9**, 1942–1950.
9 N. Hashemi, M. R. Paul, H. Dankowicz, M. Lee and W. Jhe, *J. Appl. Phys.*, 2008, **104**, 063518.
10 M. J. Fuerstman, P. Garstecki and G. M. Whitesides, *Science*, 2007, **315**(5813), 828.
11 P. Paik, V. K. Pamula and R. B. Fair, *Lab Chip*, 2003, **3**, 253–259.
12 G. I. Taylor, Low Reynolds Number Flows, National Committee for Fluid Mechanics Films, Education Development Center, Newton, MA, 1966, http://web.mit.edu/hml/ncfmf.html.
13 G. Düring, D. Bartolo and J. Kurchan, *Phys. Rev. E: Stat., Nonlinear, Soft Matter Phys.*, 2009, **79**, 030101.
14 C. Hansen, K. Leung and P. Mousavi, *Phys. World*, 2007, **20**, 24–30.
15 G. Leal, Laminar Flow and Connective Transport Processes, Butterworth-Heinemann, 1992.
16 J. P. Heller, *Am. J. Phys.*, 1960, **28**, 348–353.

17 H. Y. Tan, W. K. Loke, Y. T. Tan and N. T. Nguyen, *Lab Chip*, 2008, **8**, 885–891.
18 P. B. Howell, D. R. Mott, F. S. Ligler, J. P. Golden, C. R. Kaplan and E. S. Oran, *J. Micromech. Microeng.*, 2008, **18**, 115019–115019(7).
19 P. B. Howell, D. R. Mott, S. Fertig, C. R. Kaplan, J. P. Golden, E. S. Oran and F. S. Ligler, *Lab Chip*, 2005, **5**, 524–530.
20 P. B. Howell, J. P. Golden, L. R. Hilliard, J. S. Erickson, D. R. Mott and F. S. Ligler, *Lab Chip*, 2008, **8**, 1097–1103.
21 J. S. Kim, G. P. Anderson, J. S. Erickson, J. P. Golden, M. Nasir and F. S. Ligler, *Anal. Chem.*, 2009, **81**, 5426–5432.
22 D. C. Duffy, J. C. McDonald, O. J. A. Schueller and G. M. Whitesides, *Anal. Chem.*, 1998, **70**(23), 4974–4984.
23 T. M. Squires and S. R. Quake, *Rev. Mod. Phys.*, 2005, **77**, 977–1026.
24 K. J. Morton, K. Loutherback, D. W. Inglis, O. K. Tsui, J. C. Sturm, S. Y. Chou and R. H. Austin, *Lab Chip*, 2008, **8**, 1448–1453.
25 M. T. McBride, D. Masquelier, B. J. Hindson, A. J. Makarewicz, S. Brown, K. Burris, T. Metz, R. G. Langlois, K. W. Tsang, R. Bryan, D. A. Anderson, K. S. Venkateswaran, F. P. Milanovich and B. W. Colston, Jr, *Anal. Chem.*, 2003, **75**, 5293–5299.
26 S. Riethdorf, H. Wikman and K. Pantel, *Int. J. Cancer*, 2008, **123**(9), 1991–2006.